Pergamon

Int. J. Heat Mass Transfer. Vol. 39, No. 1, pp. 1–11, 1996

0017-9310/96 $9.50+0.00

0017-9310(95)00117-4

Laminar, buoyancy induced flow structures in a bottom heated, aspect ratio 2 duct with throughflow

STANLEY S. CHEN and ADRIENNE S. LAVINE†
University of California at Los Angeles, Los Angeles, CA 90095-1597, U.S.A.

(*Received* 16 *March* 1994 *and in final form* 10 *March* 1995)

Abstract—Three-dimensional, transient calculations have been made for flow far downstream in a horizontal, bottom heated, aspect ratio 2 duct with throughflow in the low supercritical Rayleigh number (Ra) and low Reynolds number (Re) regime. The two flow types present are longitudinal rolls and distorted, convecting transverse rolls. Longitudinal rolls results confirm previous studies. Ra and Re dependence of the transverse rolls flow field is investigated. The Nusselt number (Nu) is seen to be essentially independent of Re, and perhaps also of the flow regime. Isotherms and velocity vector plots are presented. Comparisons are made with published experimental and numerical results.

1. INTRODUCTION

Buoyant convection is present in many applications, for example, flat plate solar collectors, chemical vapor deposition (CVD) processes and cooling of electronic components. For these applications, the bottom heated layer is a model problem. A flow regime of particular interest is the regime where free and forced convection both contribute to the flow and heat transfer characteristics. Parallel rolls appear for horizontal layers when heating exceeds some critical value. Throughflow tends to align the rolls with the streamwise direction. If sidewalls are present, there is a competing mechanism that promotes the formation of rolls perpendicular to the wall and also fundamentally affects the structure of the rolls.

Building on early works studying the horizontal heated layer, throughflow effects have been studied. A good review of the literature up to the publication date of the paper is given in ref. [1]. Based on stability considerations, it can be shown that the preferred planform for low Rayleigh number (Ra) convection in a layer with throughflow is two-dimensional rolls lined up with the throughflow direction. Studies have been made of the stability of these rolls, for Couette base flow [2] and for Poiseuille base flow [3].

Sidewall effects are present in most applications. Understanding this behavior will help in assessing the agreement between experimental, theoretical and computational studies. In the no throughflow case, it was shown analytically [4] and experimentally [5] that the preferred planform is rolls lined up perpendicular to sidewalls, in particular the longer sidewalls of a finite rectangular box. These rolls are not two-dimensional rolls, but rather are three-dimensional rolls with three non-zero velocity components [6]. The geometry of interest in this paper is the horizontal, infinitely long, moderate aspect ratio duct (where aspect ratio, AR, is the ratio of the spanwise dimension of the duct, L_z^*, to the vertical dimension of the duct, L_y^*), with all walls rigid, bottom heated, top cooled and sides insulated. A linear stability analysis for this geometry [7] studied the critical Rayleigh numbers (Ra_c) for longitudinal rolls (i.e. rolls with axes along the duct axis), two-dimensional transverse rolls (i.e. rolls with axes perpendicular to the duct axis) and three-dimensional transverse roll-type structures (hereafter referred to as three-dimensional transverse rolls, or if there is no ambiguity, merely as transverse rolls). Ra_c was largest for longitudinal rolls and smallest for three-dimensional transverse rolls. This work has been confirmed experimentally [8].

Much of the research done on ducts with throughflow has concentrated on large throughflow rates, for example, the series of experimental and numerical studies by Incropera and others (e.g. [9, 10]). In contrast to the above works where the parabolized equations were used with a marching algorithm, the developing flow problem with the full three-dimensional elliptic equations was solved in ref. [11]. The spectral method and periodicity boundary conditions were used in ref. [12]. For moderate Reynolds number (Re), longitudinal rolls are seen. When Re or Gr are large enough, the rolls are not stationary. This has been seen numerically [12] and experimentally [13]. Changes in the sidewall thermal boundary conditions could induce unsteady structures that result in spanwise uniform heat or mass transfer rates. When throughflow rates are small enough, transverse rolls could appear. An extensive discussion on this subject is given in ref. [14]. Efforts to characterize this regime were reported in refs. [15, 16]. A two-dimensional

†Author to whom correspondence should be addressed.

NOMENCLATURE

AR	aspect ratio defined as L_z/L_y
g	gravitational constant
Gr	Grashof number
h	grid spacing
k	time step size
L_x	streamwise length of computational domain
L_y	height of duct, distance between heated and cooled surfaces
L_z	spanwise dimension of duct, distance between sidewalls of duct
Nu	Nusselt number
$\overline{Nu}$	average Nusselt number
P	pressure
Pe	Peclet number
Pr	Prandtl number
R	ratio of roll convective velocity to average throughflow velocity
Ra	Rayleigh number
Ra_c	critical Rayleigh number
$Ra^{\parallel}$	critical Rayleigh number for longitudinal rolls
$Ra^{\perp}$	critical Rayleigh number for transverse rolls
Re	Reynolds number
Re_t	transition Reynolds number
t	time
T	temperature
T_c	temperature of the upper, cooled duct surface
T_h	temperature of the lower, heated duct surface
u, v, w	velocity components
$\bar{u}$	average streamwise velocity
u_c	transverse roll convective velocity
u^*_{ch}	characteristic velocity, equal to α/L^*_y
x, y, z	spatial coordinates.

Greek symbols

β	volumetric coefficient of thermal expansion
κ	thermal diffusivity
λ	wavelength
ν	kinematic viscosity
ρ	density.

Subscripts

i, j, k	grid indices
max	refers to maximum value of a quantity
w	function value at a computational domain boundary.

Superscript

*	denotes dimensional quantities.

numerical study was performed for the developing flow problem for the transverse rolls regime in a heated layer with throughflow in ref. [17], and extended to three dimensions in ref. [18]. Flow was computed for larger Re and Gr in ref. [19].

2. PROBLEM STATEMENT

Low Reynolds number flow in a horizontal, bottom heated, moderate aspect ratio duct with rigid walls is studied. The coordinate axes form a right-handed system, with the origin in the lower left-hand corner of the duct: x is in the main flow direction, y in the vertical direction and z in the spanwise direction. The flow of interest is flow far from the inlet and outlet and at an asymptotic state (i.e. the structures in the flow are no longer evolving in time). AR is taken to be 2 and the Prandtl number (Pr) of the fluid to be 0.7. Past research has indicated that for a given supercritical Ra, depending on whether Re is greater than or less than a transition Re (Re_t), either longitudinal rolls or transverse rolls will appear. In this paper, first, the general behavior of the flow around Re_t is discussed. Second, characteristics of the longitudinal rolls between $Ra = 2000$ and 4000 are briefly presented. Finally, transverse rolls at $Ra = 2000$ and 4000 are studied and some comparisons made with the longitudinal rolls. The average Nu and the time averaged local Nu are compared and discussed.

3. GOVERNING EQUATIONS AND BOUNDARY CONDITIONS

The governing equations are the Boussinesq equations. The characteristic quantities used for non-dimensionalization are: distance, L^*_y; velocity, $u^*_{ch} = \kappa/L^*_y$; time, L^*_y/u^*_{ch}; pressure, ρu^{*2}_{ch}, referenced to the hydrostatic pressure at some reference temperature; temperature, non-dimensionalized with respect to the temperature difference between the heated and cooled surfaces, $(T^*_h - T^*_c)$, and referenced to the average temperature between T^*_h and T^*_c, $(T^*_h + T^*_c)/2$. The non-dimensionalized equations can be written as:

continuity

$$\frac{\partial u}{\partial x} + \frac{\partial v}{\partial y} + \frac{\partial w}{\partial z} = 0$$

momentum

$$\frac{\partial u}{\partial t} + u\frac{\partial u}{\partial x} + v\frac{\partial u}{\partial y} + w\frac{\partial u}{\partial z} = -\frac{\partial P}{\partial x} + Pr\left(\frac{\partial^2 u}{\partial x^2} + \frac{\partial^2 u}{\partial y^2} + \frac{\partial^2 u}{\partial z^2}\right)$$

$$\frac{\partial v}{\partial t}+u\frac{\partial v}{\partial x}+v\frac{\partial v}{\partial y}+w\frac{\partial v}{\partial z}$$
$$= Ra\,Pr\,T-\frac{\partial P}{\partial y}+Pr\left(\frac{\partial^2 v}{\partial x^2}+\frac{\partial^2 v}{\partial y^2}+\frac{\partial^2 v}{\partial z^2}\right)$$

$$\frac{\partial w}{\partial t}+u\frac{\partial w}{\partial x}+v\frac{\partial w}{\partial y}+w\frac{\partial w}{\partial z}$$
$$= -\frac{\partial P}{\partial z}+Pr\left(\frac{\partial^2 w}{\partial x^2}+\frac{\partial^2 w}{\partial y^2}+\frac{\partial^2 w}{\partial z^2}\right)$$

energy

$$\frac{\partial T}{\partial t}+u\frac{\partial T}{\partial x}+v\frac{\partial T}{\partial y}+w\frac{\partial T}{\partial z}=\left(\frac{\partial^2 T}{\partial x^2}+\frac{\partial^2 T}{\partial y^2}+\frac{\partial^2 T}{\partial z^2}\right).$$

The non-dimensional parameters are: $Re=\overline{u^*}L_y^*/\nu$, $Pr=\nu/\kappa$ and $Ra=g\beta(T_h^*-T_c^*)L_y^{*3}/\nu\kappa$. The $\overline{u^*}$ that Re is based on is the dimensional, average throughflow rate. The throughflow rate is specified initially, and then maintained throughout the computations.

Boundary conditions are specified as follows. For velocity, no-slip conditions are specified at the top, bottom and sides of the duct, with periodicity imposed at the inlet and the outlet of the computational domain. For temperature, T_h and T_c are specified at the bottom and top surfaces, respectively. In non-dimensional quantities, T_h is 0.5 and T_c is -0.5. The sidewalls are specified to be insulated. Periodicity is imposed on temperature at the inlet and outlet of the computational domain.

4. SOLUTION METHOD

The governing equations are solved using the finite difference method, with the diffusion terms discretized using second order centered differencing and the advective terms using a third order upwinding method [20]. The equations are integrated in time using backward Euler time integration and the discretized equations solved using the Douglas–Gunn alternating direction implicit (ADI) formalism [21]. The standard staggered grid is used. The SIMPLER method [22] is used for pressure/velocity coupling. The initial condition is specified as the Poiseuille velocity profile and the conduction temperature profile to avoid predetermining the asymptotic field planform. A random perturbation is applied to the initial temperature field as follows: for each temperature grid point, a random number between -0.5 and 0.5 is generated, multiplied by 10^{-4} and added to the initial temperature field. Greater details of the numerical formulation can be found in ref. [23].

The computational method is formally a time stepping method. When the time stepping is initiated, a time step size (k) and a limit on the number of iterations allowed within a time step is assumed. Because it is not intended to study the temporal evolution of the field, temporal accuracy is maintained only near the asymptotic state, by a suitable change of k and the number of iterations allowed within a time step.

For Re near Re_t, temporal discretization error can affect the asymptotic flow planform. When k is too large, the temporal error can cause longitudinal rolls to evolve spuriously for $Re < Re_t$ (although it never caused transverse rolls to evolve spuriously for $Re > Re_t$). Since the asymptotic field is steady and spurious transverse rolls were never observed, time stepping in the longitudinal rolls regime can be treated as a pseudo-time iterative process, and a relatively large k and small number of iterations within a time step are used. In contrast, for the transverse rolls regime, the initial k must be small enough to allow the correct flow planform to evolve. Furthermore, at the asymptotic state, since the flow is time dependent due to the rolls convecting in the streamwise direction, to obtain adequate temporal accuracy, k is reduced and iterations per time step increased. Typically, maximum residual of the governing equations and maximum dilatation less than 5×10^{-4} are maintained.

The question of the appropriate computational domain length (L_x) to specify is now discussed briefly. In the longitudinal rolls regime, the steady state is independent of x, and thus any L_x can be specified. However, in the transverse rolls regime, there is a periodicity associated with the convecting transverse rolls. L_x must be an integral multiple of a stable wavelength (λ) of the flow field or an asymptotic state will not evolve. Furthermore, unless L_x corresponds to the preferred λ, the rolls will not be of the size which would be observed experimentally. In an $AR=2$ duct, when $Re=0$, λ is close to two at $Ra_c=1842$ [7]. Since λ is a weak function of Re [8], $L_x=8$ (allowing for four pairs of rolls) was used for all $Ra=2000$ transverse rolls cases. For supercritical Ra, there is no established and accepted method for determining the preferred λ on an analytical basis [24]. The criterion selected here was the speed of evolution of the transverse rolls, an approach consistent with one that has been used in some Bénard convection studies, that is, defining the preferred λ as the one that is most unstable. Numerical experiments indicated that the rolls developed the fastest at $Ra=4000$ for $L_x=9$. This L_x has been used for all $Ra=4000$ transverse roll regime cases.

All runs have been made on an $80\times10\times20$ grid (the three numbers are the number of grid points in the x, y and z directions, respectively), the computational domain being $8\times1\times2$ for $Ra=2000$ cases, and $9\times1\times2$ for $Ra=4000$ cases. Computations have been done on the IBM 9000 at UCLA, using a double precision (64 bit arithmetic) Fortran code written to take advantage of the vector facility on the IBM 9000.

5. CODE VERIFICATION AND BENCHMARKING

The code used here was the one used to compute a related problem in ref. [25]. During the initial check-

out of the code, several exact solutions were computed to check the coding and order of accuracy of approximation. Computations made for the $10 \times 1 \times 4$ box with an $80 \times 10 \times 20$ grid for $Ra = 4000$ and $Pr = 0.71$ show good qualitative and quantitative agreement with the numerical and experimental results of ref. [26]. Temporal and spatial resolution tests were made for the present problem, for the $Ra = 4000$, $Re = 5.25$ case. Halving k resulted in a field virtually indistinguishable from the baseline solution. Computations were made on a $120 \times 15 \times 30$ grid and the vertical velocity field compared with that of the baseline. Near the sidewalls, the difference was less than 10%, and in the bulk of the domain less than 5%. This agreement is deemed to be satisfactory in light of the computationally intensive nature of the problem. Refining the grid spacing further from that used in the computations would have resulted in unacceptably large usage of computational resources.

6. GENERAL DISCUSSION OF FLOW REGIMES

Preliminary tests were made to study the nature of the flow field at low Ra and Re. A comprehensive discussion is given in ref. [14] of the flow regimes present in this problem. The critical Rayleigh numbers for longitudinal rolls and transverse rolls, $Ra^{\parallel}$ and $Ra^{\perp}$, respectively, can be found from linear stability theory [these curves are sketched in Fig. 1(a)]. $Ra^{\parallel}$ is independent of Re, but $Ra^{\perp}$ is an increasing function of Re. The portions of these two curves denoted by solid lines represent the boundary between the subcritical and the supercritical flow regimes. The portions of these curves denoted by dashed lines in Fig. 1(a) are not meaningful because they are curves generated by linear stability analyses, but actually lie in the supercritical regime.

The boundary between the transverse roll and the longitudinal roll regimes, Re_t, is a function of Ra and is in the supercritical regime. It cannot be found from linear stability analysis. It can be visualized as follows. For $Re = 0$, transverse rolls will evolve for $Ra > Ra_c$. For small Re, distorted transverse rolls are the preferred planform. However, when Re exceeds Re_t, longitudinal rolls become the preferred planform.

An attempt was made to characterize Re_t between $Ra = 1900$ and 4000. The sensitivity of the asymptotic planform type to discretization errors for Re near Re_t precluded accurate determination of the curve. Longitudinal rolls that spuriously evolved for $Re < Re_t$ (when k was too large) were indistinguishable from the true longitudinal rolls solutions for $Re > Re_t$. It should be noted that transverse rolls were never seen for $Re > Re_t$. For $Ra = 2000$, 3000 and 4000, Re_t was investigated with progressively smaller ks. The + symbols in Fig. 1(b) denote the largest Re for which transverse rolls have been seen at that Ra. The dashed line plotted below these symbols represents Re below which transverse rolls will evolve even with relatively large k. All transverse roll regime

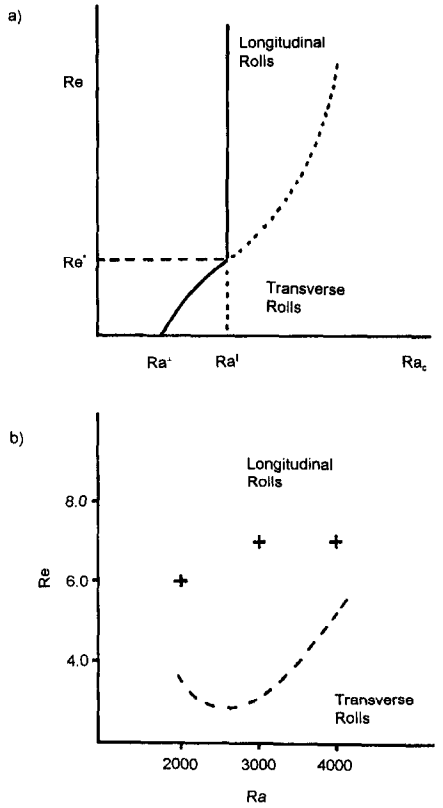

Fig. 1. Flow regimes. (a) Critical Rayleigh number as a function of Reynolds number for a finite aspect ratio duct (from Fig. VIII-15 of ref. [4]). (b) Flow map of the longitudinal roll and the transverse roll regimes: (+) the largest Re for which transverse rolls are seen at that Ra.

cases presented in this paper lie below the dashed curve. All longitudinal roll cases presented here are at $Re = 20.0$ (although cases were calculated at other Re values to verify Re independence). In ref. [15], the experimentally determined flow map for air in an $AR = 19.5$ duct indicated that Re_t should be concave downwards, as is suggested by the + data points in Fig. 1(b). There is insufficient data to make further comparisons. In ref. [16], a flow map experimentally generated for water in an $AR = 3.63$ duct revealed a flow regime that was initial-condition dependent. Perhaps some connection can be made between that flow regime and the region between the dashed curve shown in Fig. 1(b) and Re_t. A flow regime where the planform was neither longitudinal nor transverse rolls was also found in ref. [16]. In ref. [19], combined longitudinal and transverse roll type structures were found for large throughflow and heating rates. More work is necessary to characterize definitively Re_t.

7. LONGITUDINAL ROLLS REGIME

Longitudinal roll regime flow fields have been generated for Ra from 2000 to 4000 in increments of 500, for several Re at each Ra. The lower Ra limit is slightly larger than Ra_c for an $AR = 2$ duct. The upper limit

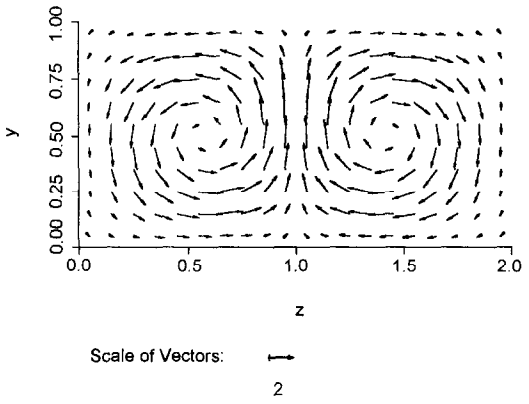

Fig. 2. Velocity vector plot for a typical y–z plane. $Ra = 2000$, $Re = 10.0$, $x = 0.05$.

was selected so that a reasonable range of $(Ra - Ra_c)$ can be studied without Ra being so large as to cause computational difficulties. Unlike previous two-dimensional or three-dimensional developing flow studies, the computations here are intended to simulate the far downstream flow in three dimensions, with periodicity boundary conditions specified at the inlet and outlet.

7.1. *Longitudinal rolls flow field characteristics*

In the longitudinal rolls regime, it is known that the flow field is steady and x independent; v, w and T are independent of Re, being functions only of Ra. In addition to being a function of Ra, u is proportional to Re. These flow characteristics were readily verified when flow fields from cases where Re is varied were compared. In the following sections, results are presented only for a single Re at each Ra.

The flow field planform is a pair of almost circular, counter rotating longitudinal rolls, with flow directed upwards at the spanwise midplane of the duct, and downwards at the sidewalls. Figure 2 shows a velocity vector plot for a representative case on a typical y–z plane. There are two possible rotational orientations for this flow planform: there could be either upflow or downflow at the $z = 1.0$ spanwise midplane. Either of these two possibilities is equally likely to result from a random initial temperature perturbation on the initial field used (a test run was made where the signs of the initial perturbation were changed and the roll orientation in the solution was reversed). To maintain a certain consistency, the same initial perturbation was used for all cases so that the rolls had the same orientation. In contrast to this study, the three-dimensional work in ref. [27] (also assuming insulated sidewalls) predicted downflow at the spanwise midplane; this was predetermined by the computational strategy used. In ref. [27], the developing flow problem is computed. Flow enters with a parabolic velocity profile, with fluid initially at T_c. As it flows downstream, the fluid near the bottom of the duct heats up. Fluid near the sidewalls is heated more than fluid near the midplane since it is slower. This establishes a tendency for fluid at the sidewalls to rise, and induces fluid at the midplane to move downwards.

Table 1(a). Longitudinal rolls regime characteristics: values of longitudinal rolls roll strength and B_v parameter for various Rayleigh number values

Ra	$\sqrt{(v^2+w^2)}$	B_v
2500	4.3043	0.1951
3000	5.9782	0.1903
3500	7.3340	0.1902
4000	8.5168	0.1911

Table 1(b). Longitudinal rolls regime characteristics: longitudinal rolls regime average Nusselt number for various Rayleigh numbers

Ra	$\overline{Nu}$
2000	1.16
2500	1.43
3000	1.63
3500	1.78
4000	1.91

7.2. *Ra dependence of the longitudinal rolls regime flow field*

When Ra is increased, there is a slight shift of the roll centers towards the upper wall and away from each other. From $Ra = 2000$ to 4000, the center of one of the rolls moves from $(y, z) = (0.5058, 0.5770)$ to $(0.5175, 0.5650)$.

A reasonable measure of the roll velocity is the l^2 norm of the velocity vector projected onto the y–z plane, i.e. $\sqrt{(v^2+w^2)}$. Table 1(a) shows the increase in this quantity with Ra. Linear theory says that roll velocity is proportional to $\sqrt{(Ra - Ra_c)}$. Writing $\sqrt{(v^2+w^2)} = B_v\sqrt{(Ra - Ra_c)}$, B_v can be computed. Since $Ra^{\parallel}$ is independent of Re, $Ra_c = Ra^{\parallel} = 2013.24$ (as obtained in ref. [7] for $Re = 0$ and $AR = 2$) has been used here. Values of B_v computed for $Ra > 2000$ [see Table 1(a)] agree with each other to within 2.5%, with an average value of 0.1917. This shows that the linear regime functional relationship holds here.

Average Nu ($\overline{Nu}$) [Table 1(b)] has been compared with the results presented in Fig. 10 of ref. [15], reproduced here as Fig. 3. The $\overline{Nu}$ computed here (marked in Fig. 3 by the + symbol) is roughly 10% greater than the experimental result of ref. [15]. The experimental results of refs. [28, 29] lie below those of ref. [15]. These three experimental studies involve ducts with large AR so it is possible that some of the differences are due to sidewall effects.

7.3. *Rayleigh number effect on streamwise velocity component and temperature*

Although increasing Ra has only a mild effect on roll shape, it dramatically increases the roll strength

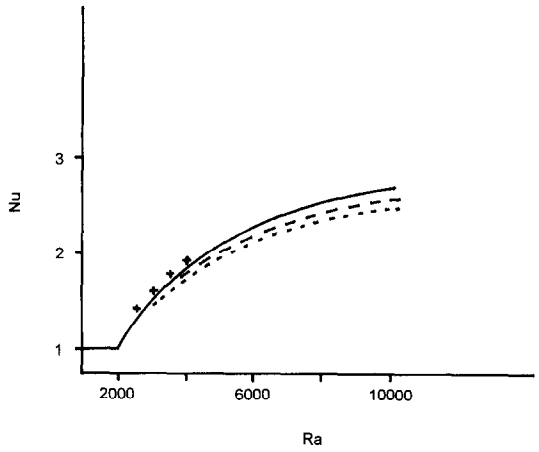

Fig. 3. *Nu* as a function of *Ra* (from Fig. 10 of ref. [15], with values from this study added): (+) computed results from this study; (——) results from ref. [15]; (– –) results from ref. [28]; (- - - -) results from ref. [29].

and the distortion of u from the unheated, Poiseuille u. A measure of this distortion is the l^2 norm of roll u (where roll u is defined as the difference between the actually computed u and the Poiseuille u). For $Ra = 2000$, this is 0.0584, increasing to 0.1581 for $Ra = 3000$ and 0.1856 for $Ra = 4000$. Note that the l^2 norm of the Poiseuille u is of the order of one. In Fig. 4(a), u as a function of y, for two zs, has been plotted for two representative cases ($Ra = 2000$, $Re = 20.0$ and $Ra = 4000$, $Re = 20.0$) together with Poiseuille u ($Ra = 0$). Heating increases flow near the top ($y = 1.0$) surface and makes u no longer symmetric with respect to the horizontal ($y = 0.5$) midplane. Plots of u and Poiseuille u as a function of z, for two ys, are presented in Fig. 4(b). Near the lower surface ($y = 0.15$), heating depresses u near the spanwise midplane ($z = 1.0$) and changes the shape of the curve markedly. Closer to the top wall ($y = 0.75$), for $Ra = 2000$, the profile of u looks like a mild perturbation of the unheated profile, but for $Ra = 4000$, substantial distortion is still seen.

Figure 5(a) and (b) show T as functions of y and z. For $Ra = 2000$, there is a relatively mild perturbation from the conduction T, but at $Ra = 4000$, the distortion is much more severe, indicating effective redistribution of the hot and cold fluid.

8. TRANSVERSE ROLLS REGIME

Transverse rolls are preferred for $Re < Re_t$. Results are presented for $Ra = 2000$ and 4000, the former being just above Ra_c, and the latter sufficiently above Ra_c so that Ra effects are clear. Three Re are computed at each Ra: $Re = 1.0$, 3.0 and 3.625 at $Ra = 2000$ and 1.0, 3.0 and 5.25 at $Ra = 4000$. These Re range from a value where the rolls are minimally distorted to where the Re effect is evident.

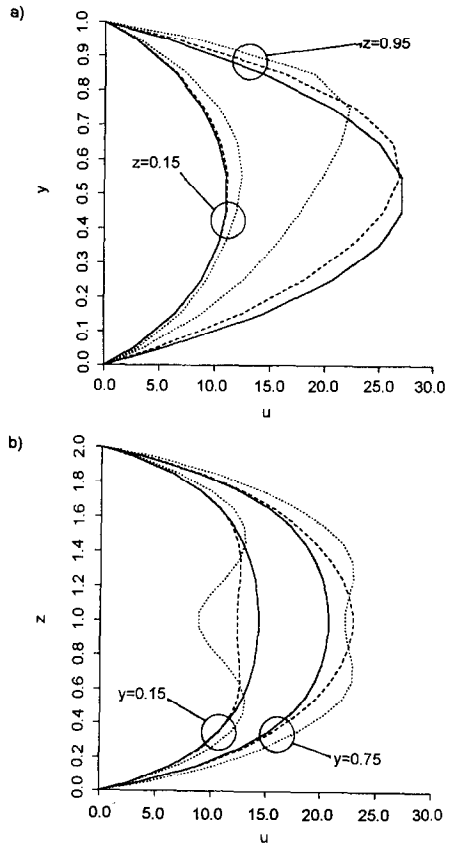

Fig. 4. u compared with Poiseuille u. (——) Poiseuille u; (– –) $Ra = 2000$, $Re = 20.0$; (- - - -) $Ra = 4000$, $Re = 20.0$. (a) As a function of y for $z = 0.15$ and 0.95. (b) As a function of z for $y = 0.15$ and 0.75.

8.1. *General features of the transverse rolls*

A fundamental difference between the longitudinal roll and the transverse roll regimes is that, in the former, a steady, fully developed state is reached; by contrast, in the latter, a far downstream, asymptotic state is attained where the distorted transverse rolls do not change form as they convect downstream with a velocity u_c (a function of Ra and Re). The flow is periodic in the streamwise direction, and any given point in the domain sees a periodic temporal variation. The differences between the two regimes underscore the competition between the wall effect, where rolls line up perpendicular to the walls, and the throughflow effect, where rolls line up with the streamwise direction.

8.2. *Detailed features of transverse rolls*

Isotherms and velocity vector plots have been developed for sections of the computational domain. Velocity vector plots for both the computed velocity and the roll velocity (i.e. the difference between computed velocity and the Poiseuille field) have been made. Plots for only a single representative section have been shown here. More results can be found in ref. [23].

Isotherms on an x–z plane ($y = 0.45$) are shown for

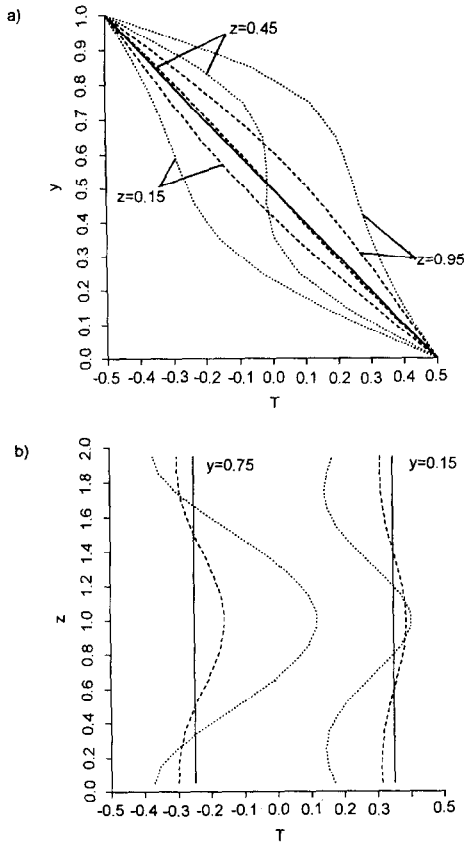

Fig. 5. T compared with conduction T. (——) Conduction T; (– – –) $Ra = 2000$, $Re = 20.0$; (- - - -) $Ra = 4000$, $Re = 20.0$. (a) As a function of y for $z = 0.15$ and 0.95. (b) As a function of z for $y = 0.15$ and 0.75.

three cases ($Ra = 2000$, $Re = 1.0$; $Ra = 2000$, $Re = 3.0$; and $Ra = 4000$, $Re = 1.0$) in Fig. 6. Consider the $Ra = 2000$, $Re = 1.0$ case [Fig. 6(a)]. The closed curves are regions of upflow and downflow, also referred to here as upward and downward jets. For the no sidewalls case, the rolls have only two non-zero velocity components (see, e.g. ref. [14]). Regions of upflow and downflow are then sheets of upward and downward moving fluid, and isotherms on x–z planes are lines perpendicular to the duct axis. With sidewalls, the rolls are three-dimensional roll type structures with a measurable w component, resulting in the upward/downward jets seen in Fig. 6(a). Boundaries between rolls are lines through the center of the jets [for example, the dashed line sketched in Fig. 6(a)]. When $Re = 0$, isotherms are symmetric about the roll centers and roll boundaries are perpendicular to the sidewalls. When Re is non-zero, the isotherms are displaced downstream [compare Fig. 6(a) and (b)].

The isotherm shapes for $Ra = 4000$, $Re = 1.0$ are different from those at lower Ra [Fig. 6(c)]. There are fewer closed curves and the isotherms look flatter, especially in the region away from the sidewalls, indicating upward/downward jets which are more sheet-like. The region of large velocity extends closer to the sidewalls since the stronger heating (higher Ra) results in rolls with larger convective velocities.

The roll center at $y = 0.5$ for a representative roll has been plotted as a function of z for each case computed (Fig. 7). For $Ra = 4000$ (dashed lines), the roll looks relatively flat away from the sidewalls. In contrast, for $Ra = 2000$ (solid lines), the wall effect extends further from the sidewalls. The distortion of the rolls is not simply proportional to Re. At $Ra = 2000$, when $Re = 1.0$, the maximum distortion is around 0.25, whereas at $Re = 3.0$, it is less than 0.6. For equal Re, distortion is smaller for larger Ra.

Isotherms for an x–y plane ($z = 0.95$) for $Ra = 2000$, $Re = 3.0$ [Fig. 8(a)] are seen to be sinusoidal type lines, in agreement with two-dimensional [15] and three-dimensional [18] developing flow numerical results. The nature of the isotherms is due to the upward/downward jets. Plots for $Ra = 4000$ show much increased 'waviness'. The rolls are well visualized by roll velocity vector plots in x–y planes [Fig. 8(b) shows a plot for $z = 0.95$ for the $Ra = 2000$, $Re = 3.0$ case]. Rolls are seen to all be the same size, with roll centers (the point where $u = v = 0$) roughly at the geometrical center of the duct half. For $Ra = 4000$, the rolls are similar, except they are slightly wider to reflect the increased $L_x = 9.0$ used (as opposed to $L_x = 8.0$ at $Ra = 2000$). The boundaries between the rolls are roughly vertical.

Total velocity vector plots on x–y planes show a different view of the rolls than roll velocity vector plots [Fig. 8(c) is such a plot for $z = 0.95$ for $Ra = 2000$, $Re = 3.0$]. The y location of the roll centers depends on the roll rotational orientation. Velocity vectors pointing downstream are larger than the ones pointing upstream. On a given x–y plane, regions around roll centers are recirculation zones. This behavior is similar to the streamlines presented in ref. [15] for two-dimensional computations.

Velocity vector plots and isotherms on x–y planes have been compared between cases with the same Ra, but different Re. For the same Ra, these fields on x–y planes look very similar. In fact, they differ only by a shift in the x direction corresponding to the roll distortion. This result can be visualized as follows. Imagine each roll to be a tube made of some elastic material and pinned to the sidewalls. For $Re = 0$, the tube is perpendicular to the sidewalls. As Re increases, the roll is more distorted by the throughflow. A cross-sectional slice of the tube in an x–y plane appears to be the same for all Re, except for a shift in the downstream direction. In this sense, one can think of the buoyancy and shear effects as being additive. This apparent decoupling of the two effects explains the fact that average Nu ($\overline{Nu}$) is substantially independent of Re. It also explains why parameters such as u_c and $\overline{Nu}$ from two-dimensional results correlate well with those from three-dimensional results.

By tracking the movement of the center of a representative roll, u_c can be inferred. For all cases computed, $R = u_c/\bar{u}$ (where $\bar{u}$ is the non-dimensional aver-

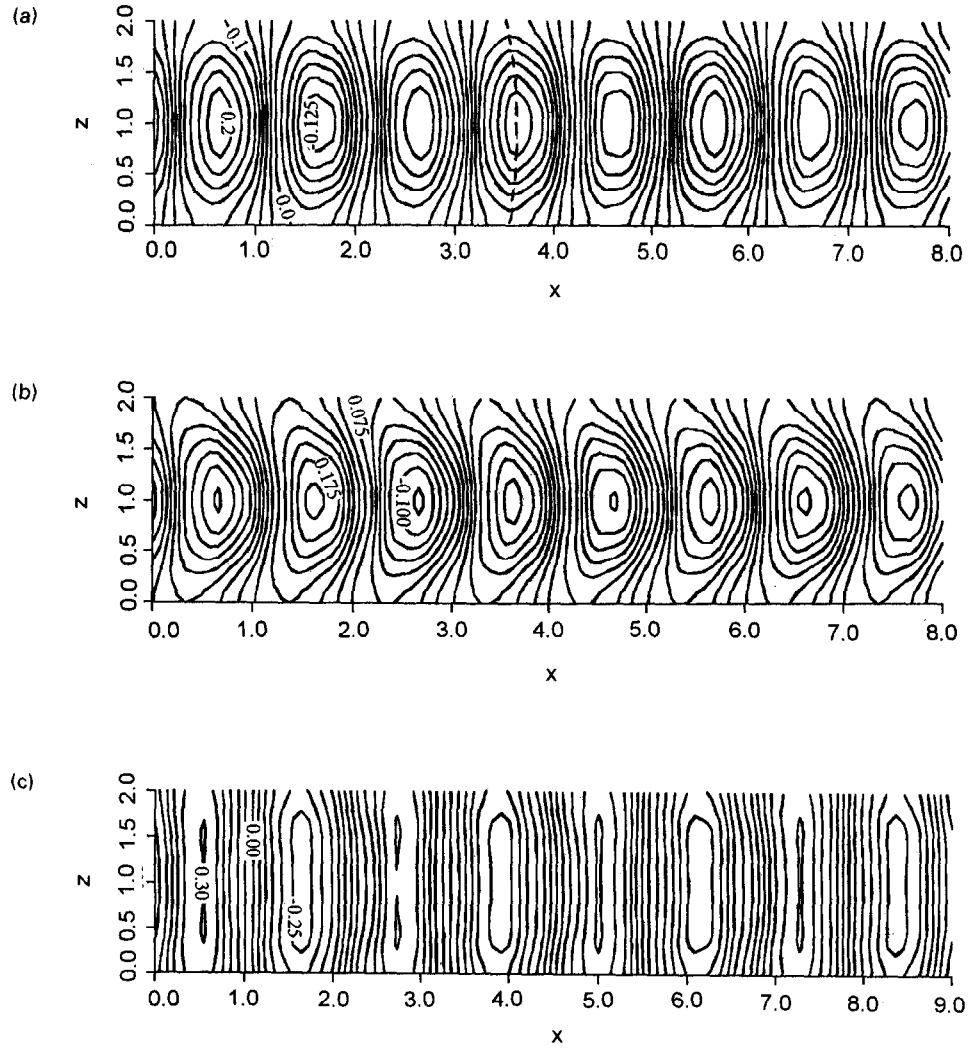

Fig. 6. Isotherms for an x–z plane at $y = 0.45$: (a) $Ra = 2000$, $Re = 1.0$ (isotherms $\Delta T = 0.025$ apart); (b) $Ra = 2000$, $Re = 3.0$ (isotherms $\Delta T = 0.025$ apart); (c) $Ra = 4000$, $Re = 1.0$ (isotherms $\Delta T = 0.05$ apart).

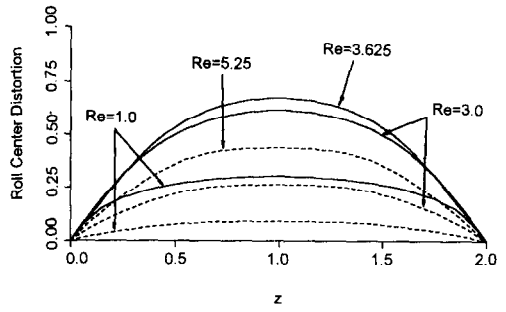

Fig. 7. Roll center distortion as a function of Re: (——) $Ra = 2000$; (- - - -) $Ra = 4000$.

age throughflow velocity, equal to $Re\ Pr$) has been found. R values for $Ra = 2000$ cases agree to less than 1% and for $Ra = 4000$ to less than 3%, confirming the Re independence of R [30]. At $Ra = 2000$, $R = 1.32$ and at $Ra = 4000$, $R = 1.13$. These R values have been plotted with the results presented in Fig. 5 of ref. [30] (Fig. 9). The two-dimensional numerical results of ref. [30] show R to be relatively Ra independent. The two-dimensional numerical results of ref. [15] lie above that of ref. [30], and show R slightly decreasing with Ra. The experimental results of ref. [15] (air in an $AR = 19.5$ duct) lie between the two curves mentioned above, and also show R decreasing with Ra. The R values computed here lie between the numerical work of ref. [30] and the experimental results of ref. [15]. The single case computed in ref. [17] in the three-dimensional developing flow calculations agrees well with the two-dimensional numerical results of ref. [30].

$\overline{Nu}$ has been computed for all cases and is seen to be substantially Re independent (Table 2). Recalling that the $\overline{Nu}$ values for $Ra = 2000$ and 4000 in the longitudinal rolls regime are 1.16 and 1.91, respectively, it is seen that $\overline{Nu}$ is at most a weak function of the flow regime.

The time averaged local Nu, referred to here as the

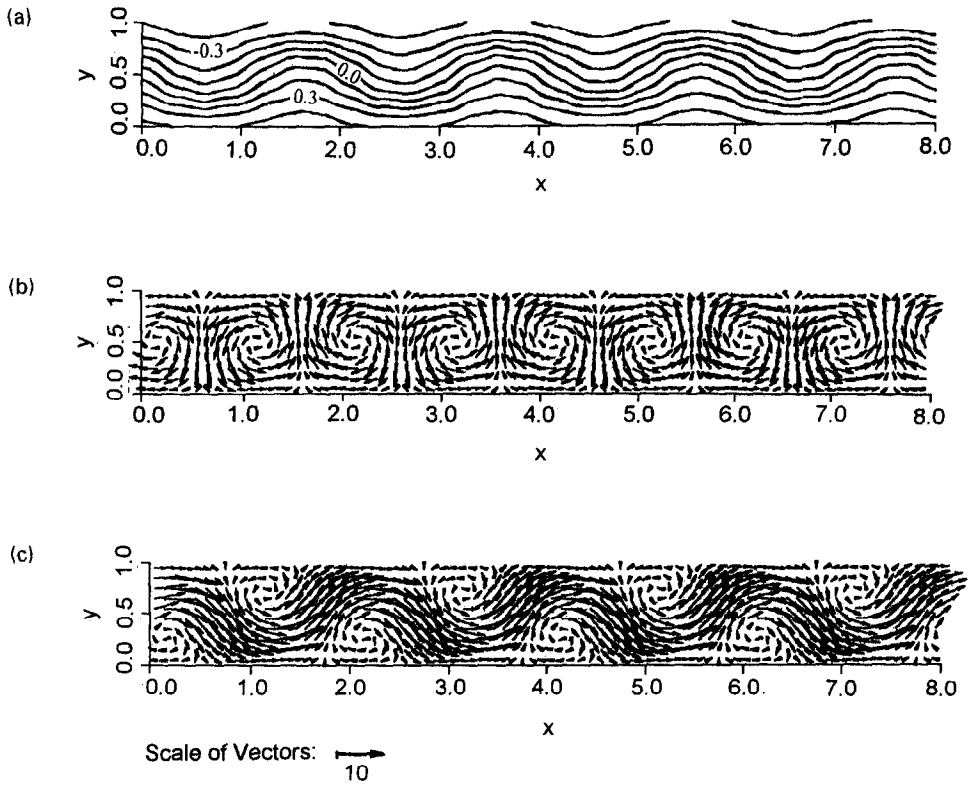

Fig. 8. Isotherms and velocity vector plots for an x–y plane at $z = 0.95$. $Ra = 2000$, $Re = 3.0$. (a) Isotherms ($\Delta T = 0.1$ apart). (b) Roll velocity vector plot. (c) Total velocity vector plot.

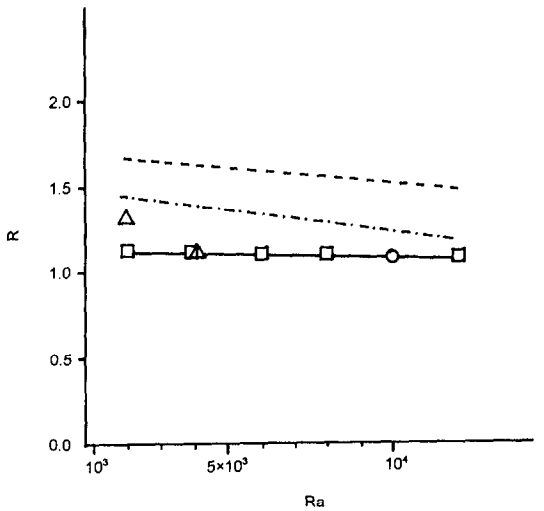

Fig. 9. Roll convective velocity (from Fig. 5 of ref. [30] with values from this study added): (△) results from present study; (□) results from ref. [30]; (○) results from ref. [17]; (– – –) results from ref. [15] (numerical); (– · – · –) results from ref. [15] (experimental).

local Nu, has been computed for the top and bottom walls and compared with that for the longitudinal rolls regime (Fig. 10 shows the $Ra = 4000$ case). Because of the temporally and spatially periodic nature of the transverse rolls regime flow field, the time averaged and the space averaged local Nu are the same and are

Table 2. Transverse rolls regime average Nusselt number

Re	$\overline{Nu}$
$Ra = 2000$	
1.0	1.11
3.0	1.09
3.625	1.08
$Ra = 4000$	
1.0	1.77
3.0	1.76
5.25	1.74

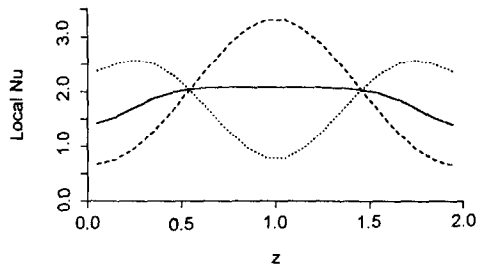

Fig. 10. Comparison of local Nusselt number for $Ra = 4000$ between the transverse roll and the longitudinal roll regimes: (——) transverse rolls regime ($Re = 5.25$); (– – –) longitudinal rolls regime, upper wall; (- - - -) longitudinal rolls regime, lower wall.

a function only of z. The longitudinal rolls flow field is x independent, so local Nu is also a function only of z. Only a single curve is plotted for the transverse rolls regime local Nu because it is essentially Re independent and the same at the top and bottom walls. In the region away from the sidewalls, local Nu is almost constant, this region being smaller for $Ra = 2000$ (not shown). The local Nu for the longitudinal rolls regime is distinctly different. The top and bottom wall local Nus are different. There is substantial spanwise variation, with minimum Nu and maximum Nu differing by more than 100%. The local Nu curves can be explained in the context of the different planform types of the two flow regimes. In the longitudinal rolls regime, upflow at the $z = 1.0$ midplane brings hot fluid to the cold wall; near the sidewalls, downflow brings cold fluid to the lower wall. Since the rolls are stationary, this results in localized regions of enhanced heat transfer. In contrast, rolls in the transverse rolls regime have axes essentially along the z direction and convect down the duct. Thus, time averaging eliminates variations due to upflow and downflow, leaving only variations due to the side boundary layer. For applications such as CVD, it is necessary to have spanwise uniform mass transfer, as will be the case if the time averaged Nu is uniform. The transverse rolls regime is desirable in this context. However, Re and Ra values for most applications are large, so manipulation of parameter values or sidewall conditions to produce unsteady flow [13] is more realistic.

9. SUMMARY AND CONCLUSION

The bottom heated, aspect ratio 2 duct with throughflow was studied for the low Ra and low Re regime. The Ra range investigated was 2000–4000, from slightly above Ra_c to approximately twice critical. The Re range was 1.0–20.0, spanning the longitudinal rolls and the distorted, convecting transverse rolls flow regimes. Unlike previous two-dimensional fully developed or three-dimensional developing flow studies, the far downstream flow is simulated in three dimensions here.

Preliminary investigations were made for flow near Re_t. Sensitivity of the flow planform to numerical error hampered the effort to characterize Re_t. Longitudinal rolls spuriously evolved for $Re < Re_t$ unless time stepping was initiated with a sufficiently small k to ensure that temporal error was small.

Results in the longitudinal rolls regime are in agreement with known results: flow is steady and independent of the streamwise direction, with the secondary flow and T independent of Re; u is seen to be proportional to Re. Heating shifts the y coordinate of maximum u upwards, and increases the flow rate near the sidewalls at the expense of flow near the $z = 1.0$ midplane. T is distorted from the linear conduction profile.

The transverse rolls regime for $Ra = 2000$ and 4000 was studied. Isotherms and velocity vector plots for two-dimensional sections of the computational domain were generated. Throughflow distorts the rolls by an amount that increases with Re and decreases with Ra. For $Ra = 2000$, the distortion of the roll is distributed over the entire duct, whereas for $Ra = 4000$, the distortion is more localized near the sidewalls. Substantial decoupling of the buoyancy and shear effects is seen, that is, the flow at each x–y plane is seen to be essentially independent of Re, with the structures being identical up to a shift reflecting the distortion of the rolls. The average Nu and the time averaged local Nu appear to be independent of Re and perhaps of flow regime also, and a function only of Ra. The spanwise distribution of the local Nu is strongly z dependent in the longitudinal rolls regime, but only a weak function of z in the transverse rolls regime except in the region near the sidewalls. The ratio of the convective velocity of the rolls to the average throughflow velocity is seen to be a function only of Ra. Computed values of the ratio are within 10% of published two-dimensional numerical results, and within 20% of published experimental results.

Acknowledgement—The authors would like to thank Dr Tien-Chien Jen for his assistance with the figures.

REFERENCES

1. R. E. Kelly, The onset and development of thermal convection in fully developed shear flows. In *Proceedings of the 9th International Heat Transfer Conference* (Edited by G. Hestroni), pp. 35–112. Hemisphere, Washington, DC (1990).
2. R. M. Clever, F. H. Busse and R. E. Kelly, Instabilities of longitudinal convection in Couette flow, *Z. Angew. Math. Phys.* **28**, 771–783 (1977).
3. R. M. Clever and F. H. Busse, Instabilities of longitudinal rolls in the presence of Poiseuille flow, *J. Fluid Mech.* **229**, 517–529 (1991).
4. S. H. Davis, Convection in a linear box: linear theory, *J. Fluid Mech.* **30**, 465–478 (1967).
5. K. Stork and U. Müller, Convection in boxes: experiments, *J. Fluid Mech.* **54**, 599–611 (1972).
6. R. P. Davies-Jones, Thermal convection in an infinite channel with no-slip sidewalls, *J. Fluid Mech.* **44**, 695–704 (1970).
7. J. M. Luijkx and J. K. Platten, On the onset of free convection in a rectangular channel, *J. Non-Equilib. Thermodynam.* **6**, 141–158 (1981).
8. J. M. Luijkx, J. K. Platten and J. Cl. Legros, Precise measurements of the wavelength at the onset of Rayleigh–Bénard convection in a long rectangular duct, *Int. J. Heat Mass Transfer* **25**, 1252–1254 (1982).
9. F. P. Incropera, A. L. Knox and J. R. Maughan, Mixed-convection flow and heat transfer in the entry region of a horizontal rectangular duct, *ASME J. Heat Transfer* **109**, 434–439 (1987).
10. H. V. Mahaney, F. P. Incropera and S. Ramadhyani, Development of laminar mixed convection flow in a horizontal rectangular duct with uniform bottom heating, *Numer. Heat Transfer* **12**, 137–155 (1987).
11. T. A. Nyce, J. Ouazzani, A. Durand-Daubin and F. Rosenberger, Mixed convection in a horizontal rectangular channel—experimental and numerical velocity distributions, *Int. J. Heat Mass Transfer* **35**, 1481–1494 (1991).
12. I. Hosokawa, Y. Tanaka and K. Yamamoto, Mixed convective flow with mass transfer in a horizontal rec-

tangular duct heated from below simulated by the conditional fourier spectral analysis, *Int. J. Heat Mass Transfer* **36,** 3029–3042 (1993).
13. H. Koizumi and I. Hosokawa, Unsteady behavior and mass transfer performance of the combined convective flow in a horizontal rectangular duct heated from below, *Int. J. Heat Mass Transfer* **36,** 3937–3947 (1993).
14. J. K. Platten and J. C. Legros, *Convection in Liquids*. Springer, Berlin (1984).
15. M. T. Ouazzani, J. P. Caltagirone, G. Meyer and A. Mojtabi, Etude numérique et expérimentale de la convection mixte entre deux plans horizontaux à température différentes, *Int. J. Heat Mass Transfer* **32,** 261–269 (1989).
16. M. T. Ouazzani, J. K. Platten and A. Mojtabi, Etude expérimentale de la convection mixte entre deux plans horizontaux à température différentes—II, *Int. J. Heat Mass Transfer* **32,** 261–269 (1989).
17. G. Evans and R. Greif, A study of traveling wave instabilities in a horizontal channel flow with applications to chemical vapor deposition, *Int. J. Heat Mass Transfer* **32,** 895–913 (1989).
18. G. Evans and R. Greif, Unsteady three dimensional mixed convection in a heated horizontal channel with applications to chemical vapor deposition, *Int. J. Heat Mass Transfer* **34,** 2039–2051 (1991).
19. G. Evans and R. Greif, Thermally unstable convection with applications to chemical vapor deposition channel reactors, *Int. J. Heat Mass Transfer* **36,** 2769–2782 (1993).
20. R. K. Agarwal, A third-order-accurate upwind scheme for Navier–Stokes solutions at high Reynolds numbers, Paper AIAA-81-0112, AIAA 19th Aerospace Sciences Meeting, St Louis, MO (1981).
21. J. Douglas and J. E. Gunn, A general formulation of alternating direction methods. Part I. Parabolic and hyperbolic problems, *Numer. Math.* **6,** 428–453 (1964).
22. S. V. Patankar, *Numerical Heat Transfer and Fluid Flow*. Hemisphere, Washington, DC (1980).
23. S. S. Chen, Buoyancy induced flow structures in a bottom heated, aspect ratio two, duct with throughflow, Ph.D. Dissertation, University of California, Los Angeles, CA (1993).
24. I. Catton, Wavenumber selection in Bénard convection, *ASME J. Heat Transfer* **110,** 1154–1165 (1984).
25. S. S. Chen, A. S. Lavine and J. M. McDonough, Computations of three-dimensional opposing mixed convection between inclined heated plates, *Proceedings of the Ninth International Heat Transfer Conference*, Vol. 2, pp. 291–296. Jerusalem (1990).
26. K. R. Kirchartz and H. Oertel, Jr, Three-dimensional thermal cellular convection in rectangular boxes, *J. Fluid Mech.* **192,** 2249–2286 (1988).
27. H. K. Moffat and K. F. Jensen, Three-dimensional flow effects in silicon CVD in horizontal reactors, *J. Electrochem. Soc.* **135,** 459–471 (1988).
28. K. Fukui, M. Masamoto and H. Ueda, The longitudinal vortex and its effect on the transport processes in combined free and forced laminar convection between horizontal and inclined parallel plates, *Int. J. Heat Mass Transfer* **27,** 109–120 (1983).
29. S. Ostrach and Y. Kamotani, Heat transfer augmentation in laminar fully developed channel flow by means of heating from below, *ASME J. Heat Transfer* **97,** 220–225 (1976).
30. M. Hasnaoui, E. Bilgen, P. Vasseur and L. Robillard, Mixed convective heat transfer in a horizontal channel heated periodically from below, *Numer. Heat Transfer, Part A* **20,** 297–315 (1991).